

This is the accepted version of this paper.

The version of record can be accessed at <https://doi.org/10.1680/jphmg.21.00080>

ABSTRACT

Shafts are frequently constructed to allow access to subsurface infrastructure and the resulting excavation generally deep and narrow. Shafts may be constructed using a variety of methods and plan forms dependent on ground conditions and intended use. An axisymmetric (cylindrical) geometry is often preferred due to the relatively simple structural analysis, construction method and for a number of approaches that are available to estimate the ground movements around such an excavation. In certain cases, particularly when there is restricted space both above and below surface, non-circular shafts could be a preferred solution. The assessment of surface movements around non-circular shafts is difficult as little information exists and there are few empirical prediction methods available. In this study, a series of centrifuge tests have been conducted to investigate the effects of modifying the cross-sectional profile of a shaft (i.e. circular in plan compared with elliptical). Analysis of measurements obtained from centrifuge tests undertaken at City, University of London's geotechnical centrifuge facility are presented and compared with existing predictive methods. An addendum to the empirical equations and procedures for predicting surface settlements arising from circular shafts is presented to allow for the assessment of movements around elliptical shafts in clay.

KEYWORDS

Shaft construction; Ground movements; Centrifuge modelling

LIST OF SYMBOLS

a	Constant indicates the depth at which maximum horizontal displacement occurs
b	Constant governs the height of the Gaussian curve
d	Distance from the shaft wall
D	Shaft diameter
H	Shaft depth
K_0	The ratio between horizontal and vertical effective stresses at rest
OCR	Overconsolidation ratio
n	Multiple of shaft depth, H , to a distance, d , from the shaft wall where settlement becomes zero
PIV	Particle Image Velocimetry
PPT	Pore Pressure Transducer
S_v	Vertical soil displacement
S_h	Horizontal soil displacement
S_u	Undrained shear strength of clay
α	Empirical constant
ϕ'_c	Critical state angle of shearing resistance
σ'_h	Horizontal effective stress
σ'_v	Vertical effective stress
σ'_{v0}	Maximum consolidation pressure for clay model in centrifuge test
z	Depth below soil surface

1 INTRODUCTION

2

3 In a developed urban environment the surface space is heavily utilised leading engineers to
4 develop tunnelling solutions for housing transport links, water services, sewage services,
5 communication networks and electrical lines. Access to these tunnelling systems can be a
6 considerable challenge, particularly for transportation systems where easy access is required for
7 thousands of people daily. There are many solutions to this problem of access including the
8 sinking of shafts to intersect with tunnels or other structures (such as stations) below. The
9 construction of a deep shaft will generate ground movements driven by reduction of horizontal
10 stresses on the soil around the shaft and vertical stresses at the base but also influenced by other
11 factors such as method of shaft construction, workmanship and dewatering. In a dense urban
12 environment these movements have the potential to cause structural damage to existing surface
13 and subsurface infrastructure and this must be, at the design stage, assessed.

14 The most common geometric form of a shaft is circular in plan cross-section. This shape is
15 favoured due to the inherent advantage of radial symmetry. In this case the analysis of the lining
16 can assume that loads are carried by the stiff hoop and that any ground movements generated
17 during construction will be radially symmetric both above and below the ground surface. These
18 assumptions do not, of course, account for variations in the soil around the shaft or construction
19 methods and tolerances (potentially leading to non-uniform pressures being applied to the lining
20 and non-uniform ground movement) or the presence of any existing buildings which would also
21 contribute to asymmetric behaviour.

22 In theory a shaft can be sunk with any cross-sectional geometry. There are obvious
23 disadvantages to certain shapes (e.g. a square or rectangular shaft would require a stiff design
24 at the corners of the lining to counter the bending moments generated by the pressure acting on
25 the sides) but there are advantages to an elliptical cross-section particularly in cases of restricted
26 surface space (e.g. Feiersinger, 2011). Figure 1 shows a sketch of a hypothetical project to install
27 two lifts for underground access to a metro station. The lifts are represented by the squares and
28 the required circular or elliptical shaft to house them is shown. For this particular (notional)
29 geometry the elliptical shaft has a plan area that is approximately 25% smaller which would have
30 significant benefit in terms of removal of spoil from site. Additionally, the elliptical geometry could

31 be aligned in such a way so as to avoid any surface or subsurface structures that may already
32 exist. Taking into account these potential benefits, the objective of this paper is to provide
33 experimental data on elliptical shaft construction in clay to support current design methodologies.

34

35 SHAFT DESIGN AND CONSTRUCTION

36

37 Construction of a shaft in clay can be carried using a number of methods dependent on the
38 strength of the clay. Allenby & Kilburn (2015) discuss shaft-sinking techniques divided into two
39 general categories; underpinning and caisson sinking however Schwamb (2014) also highlights
40 the use of piling and diaphragm walling as viable construction techniques. In an urban
41 environment where there are limitations on available space, noise and vibrations, shafts are
42 usually constructed by underpinning (e.g. Morrison *et al.*, 2004). Underpinning is a construction
43 technique which incrementally excavates the shaft followed by installation of a pre-cast concrete
44 segmental lining and grouting behind the annulus (Allenby & Kilburn, 2015). There are also recent
45 examples of shaft construction in stiff clays using a sprayed concrete lining (e.g. Rutty *et al.*, 2015)
46 which also use an underpinning method. It is worth highlighting this technique as its flexibility
47 would make it most suitable for construction of non-circular geometries. When utilising sprayed
48 concrete, excavation is followed by construction of a primary lining (using sprayed concrete) which
49 is then supplemented by a secondary lining constructed soon after (usually Cast-in-place or pre-
50 cast concrete). The primary lining can be assumed to carry none of the load in the long term (as
51 in Rutty *et al.*, 2015) or it can work with the secondary lining (as in Psomas *et al.*, 2019).

52 Modern geotechnical engineering practice aims to reduce ground movements arising from
53 construction to a minimum. BS EN 1997-2:2007 (BSI, 2007) specifies that the design of a shaft
54 (of any cross-section) must include detailed assessments of the adjacent ground movements in
55 order to assess any impact on existing structures. There is little guidance available to aid with
56 these assessments although, most notably, New & Bowers (1994) give a prediction method for
57 surface settlements arising from circular shaft sinking in London clay (recently updated; New,
58 2017). In this work it is asserted that predictions can only be made by referring to field data in
59 similar soil conditions but these data are relatively limited in the literature, particularly so when
60 compared with those of other geotechnical construction events (i.e. tunnelling). Le *et al.* (2019)

61 extends this work to subsurface movements but again, the field data with which to validate these
62 methods is limited.

63 When considering an elliptical shaft, it may be possible to adapt the work of New (2017) with
64 additional modifications or assumptions in order to generate surface settlement predictions.
65 Alternatively, finite element methods could be used to make predictions of ground movements
66 (e.g. Pedro *et al.*, 2019) but observational data are vital for validating any numerical analysis of
67 elliptical shaft excavations. There are very few published case studies reporting the construction
68 of and the ground movements arising from elliptical shafts. Feiersinger (2011) reports the
69 construction of a lift shaft at Green Park station in London using a sprayed concrete primary lining
70 and cast-in-place secondary linings and whilst some information is given on instrumentation that
71 was installed for surface movements, the measurements reported concentrate on the influence
72 of the shaft on existing subsurface assets such as escalators and tracks. The shaft is
73 approximately 27m deep with a major and minor axis of 8.6m and 5.6m respectively in the upper
74 10m widening to a major and minor axis of 10m and 6.2m for the remaining depth. Topa Gomes
75 *et al.* (2008) report a shaft construction based on two overlapping ellipses in a relatively
76 uncongested urban space. Some subsurface movements are presented but relatively close to
77 the shaft walls. In general, there is a lack of reported case data on which to base future
78 assessments.

79

80 GROUND MOVEMENTS ARISING FROM SHAFT CONSTRUCTION

81

82 Ground movements generated by shaft construction will comprise vertical settlements and
83 horizontal movements towards the shaft. These are primarily driven by reductions in horizontal
84 and vertical earth pressures however, as Faustin (2017) identifies, there are many factors that
85 contribute to the overall movements both in the short and the long term. These include (but are
86 not limited to) the diameter and depth of the shaft, the construction method employed,
87 workmanship, ground conditions and other processes such as dewatering or consolidation.

88 The vertical surface settlements arising from sinking a circular shaft in stiff London Clay during
89 the Heathrow Express Trial Tunnel were reported by New & Bowers (1994) and used to establish

90 **Equation 1.**

$$S_v = \alpha H \left(1 - \frac{d}{H}\right)^2 \quad (1)$$

91 Where S_v is the surface settlement at a distance, d , behind the wall. H is the depth of shaft and
92 α is an empirical constant that depends on ground conditions and construction method (in the
93 original work α had a value of 6×10^{-4}). The limitations of **Equation 1** are that the diameter of
94 excavation is not considered and there is a level of uncertainty surrounding the value of α .

95 Subsequently, New (2017) documented field data from thirteen case studies with a wide range of
96 diameters (although predominantly in stiff London Clay). An amendment to **Equation 1** was
97 proposed with a new variable, n , controlling the extent of the vertical settlements around the
98 excavation (**Equation 2**).

$$S_v = \alpha H \left(1 - \frac{d}{nH}\right)^2 \quad (2)$$

99 Whilst there is still no explicit term considering the diameter of the shaft, the data presented by
100 New (2017) clearly shows that larger shafts produce (as might be expected) larger settlements
101 over a greater extent. It might also be logical that softer soils would produce larger movements,
102 an observation supported by the experimental data from Le *et al.* (2019).

103 As noted earlier, there is limited published data in the literature reporting either field
104 measurements, experimental data or numerical analyses of shaft construction. When considering
105 elliptical shafts the available literature is even more restricted however, Faustin *et al.* (2018) report
106 a series of centrifuge tests on model elliptical shaft excavations in sand. These tests modelled a
107 1:80 scale elliptical shaft excavation (with equivalent prototype dimensions of major axis length =
108 14.4m, minor axis length = 9.6m and excavation depth 15.4m) in Fraction E Leighton Buzzard
109 Sand with a stiff aluminium liner. The measurements during these tests were of the surface
110 settlement and lining strains. The surface settlement data was compared with those from tests
111 on circular shafts and showed that the maximum settlement was slightly higher in the elliptical
112 shaft excavation (0.028%H compared with 0.02%H). However, it should be noted that these
113 measurements may not be directly comparable as the plan area of the elliptical shaft modelled is
114 larger than that of the circular shaft. Faustin *et al.* (2018) also state that the extent of the surface
115 settlements is larger for the circular shaft when compared with the elliptical shaft (1.5H compared

116 with 1.0H) however the data presented do not necessarily support this rather more measurements
117 are reported for the circular tests at a greater distance from the shaft.

118 It is clear that, accepting that elliptical shaped shafts are likely to be utilised in future construction
119 projects, there is a need to understand and predict the movements generated during their
120 excavation. A series of centrifuge tests to examine this are now described.

121

122 CENTRIFUGE TESTING

123

124 Novel apparatus was developed to model the ground movements induced by a circular shaft
125 excavation in overconsolidated clay (Divall & Goodey, 2016). In that work, good agreement was
126 shown between the data collected from experiments using this apparatus and the prediction
127 methods of New (2017). This apparatus does not model the soil-structure interaction between
128 the soil and the shaft liner but rather it generates ground movements by allowing a small gap
129 between the soil and a solid former to close, analogous to the volume loss that might be observed
130 during tunnel excavation. The rationale for this experimental approach is to remove any influence
131 of liner stiffness and concentrate solely on the patterns of ground movement. Based upon the
132 designs described by Divall & Goodey (2016), modifications were made to the apparatus for
133 modelling elliptical shafts whilst using an identical test procedure.

134

135 *Test apparatus*

136 A basic apparatus schematic of the shaft centrifuge models is given in Figure 2. In this series of
137 experiments, all excavations are modelled as half-space simulations. This allows measurements
138 of soil movement to be made using digital analysis of images taken of the experiment through a
139 Perspex window on one side of the container. This would not be possible if the experiments
140 utilised a full model of the shaft. The finished model comprises a consolidated clay sample with
141 a pre-cut excavation, into which is placed an apparatus supporting that excavation during in-flight
142 consolidation which then allows simulation of the shaft construction once the groundwater
143 conditions are established.

144 The apparatus comprises a fully solid former enclosed within a latex bag. This solid former is
145 used instead of a thin hollow liner to support the soil in its final position as, in these experiments

146 where only half of the shaft is modelled, use of a thin liner would incorrectly represent the
147 boundary condition at the edges in the plane of the cut. At the very base of the former, there is a
148 small cavity which allows for basal heave to develop as the vertical stress is relieved during the
149 excavation simulation. In this area the former is more representative of the real case but the wall
150 is sufficiently thick to minimise bending. This apparatus is suspended from a stiff bracket attached
151 to the upper surface of the box containing the experiment. The former is sized such that when
152 installed within the pre-cut shaft excavation, there is a 4.5mm annular gap between the clay and
153 the outer face of the former. The latex bag has a thickness of 1.5mm and, as such, when
154 assembled there is a uniform 3mm gap around the annulus of the model. This gap can be
155 considered to represent the amount of overcutting that might occur during excavation and the
156 former to be the final position of the (e.g.) precast shaft lining. Thus, in the experiment,
157 movements are driven by the closing of this annular gap. The amount of overcutting modelled
158 here (300mm at prototype scale) is relatively large (100mm might be expected in practice). The
159 choice of a 3mm gap is driven by the need to generate movements large enough to measure
160 however the resulting measurements are normalised for comparison with other experiments or
161 case studies. The void between former and latex bag (which includes the cavity at the base) is
162 filled with a heavy fluid (sodium polytungstate) which has a bulk unit weight equivalent to that of
163 the surrounding soil. This heavy fluid supports the clay both around the shaft and at the formation
164 level during centrifuge flight whilst the pore pressures in the soil reached hydrostatic equilibrium
165 with a water table set by a standpipe (at the ground surface) outside the model. Simulation of
166 construction is then effected by draining the heavy fluid from the base of the latex bag which
167 simultaneously reduces the horizontal stresses at the shaft perimeter and the vertical stress at
168 formation level. Figure 3 shows the apparatus, how it sits within the clay model and how it
169 attaches to the box within which it sits. More details of the model apparatus setup (for the
170 reference case circular shaft geometry) are given in Le *et al.* (2019).

171 The two model elliptical shafts (shown in Figure 2) had plan cross-sectional areas equal to the
172 circular shaft which is used as a reference case and is of the same dimensions as that described
173 by Le *et al.* (2019) which is of 8m diameter and 20m depth at prototype scale, but had major and
174 minor axes chosen to represent an approximately similar aspect ratio to the lower section of the
175 elliptical shaft constructed at the Green Park underground station upgrade in London, UK

176 (Feiersinger, 2011). The tests were conducted at 100g and thus the model elliptical shaft had a
177 minor axis of 64mm, a major axis of 100mm and a depth of 200mm, the slight variation between
178 this and the prototype size being due to the requirement of the plan area being the same as the
179 circular reference case. It should be noted that both apparatus representing the elliptical shafts
180 have the same dimensions but have their plane of symmetry (in the model) corresponding with
181 either the major or the minor axis. This approach allows a modelling of models scenario and
182 enables investigation of the two different ground movement measurement techniques (detailed
183 later).

184

185 *Test series*

186 A total of three tests were completed during this work. All three clay samples used in the tests
187 were consolidated to 350kPa and swelled to 250kPa. All samples underwent further in-flight
188 consolidation on the centrifuge resulting in samples that had varying strength and
189 overconsolidation ratio with depth. The tests can be separated into two categories; CR, the
190 reference circular shaft simulation and EL1 & EL2, the two different elliptical shaft simulations.
191 Details of these test are summarised in Table 1. Where H is the depth of excavation, h is the
192 horizontal axis length (i.e. the dimension across the box), v is the vertical axis length (the
193 dimension into the box) and A is the cross-sectional area of the model shafts.

194

195 *Test procedure and instrumentation*

196 The soil samples were created by mixing Speswhite kaolin powder, a clay whose engineering
197 properties are well-established for centrifuge modelling (Grant, 1998), with distilled water to a
198 form a slurry with a water content of 120% (twice the liquid limit). This slurry was placed within a
199 soil container, known as a strongbox, and subjected to a vertical effective stress history as
200 detailed previously. This process took approximately one week. During the swelling stage, two
201 pore-water pressure transducers were installed via the back wall of the strongbox, the primary
202 function of which is to ensure that pore water pressure within the soil achieves equilibrium with
203 the standpipe during the in-flight consolidation phase.

204 Once the clay sample is prepared, the model making procedure would begin more details on
205 which can be found in Le *et al.* (2019). The main aspects are briefly described below:

-
- 206 • The front wall of the strongbox was removed and the exposed surfaces of the clay sample
207 were sealed with silicone oil to prevent drying out,
 - 208 • The soil sample was trimmed to the desired model height (275mm) and the semi-
209 elliptical/circular cavity was manually cut into the front face of the clay sample using a
210 specially constructed cutter and guide,
 - 211 • This front face of the model was sprayed with dyed blue Leighton Buzzard Sand (Fraction
212 B) whereas the top of the model was sprinklered with Leighton Buzzard Sand (Fraction E)
213 to create the texture necessary for post-test image analysis of soil movement,
 - 214 • The 83mm thick PMMA (Poly(methyl methacrylate)) window was bolted to the front of the
215 strongbox which had the model shaft elements already attached,
 - 216 • The drainage channels were connected and the gantry necessary for 3D topography (Le
217 *et al.*, 2016) was bolted to the top of the strongbox (Figure 3), and finally,
 - 218 • The latex bag was filled with the heavy fluid and all air bled out of the system.

219

220 The model was placed on the centrifuge swing (City, University of London has access to an
221 Acutronic 661 and a description of the main features can be found in Panchal, 2018) and
222 accelerated to 100g. The model was kept at this acceleration until the clay had reached
223 hydrostatic equilibrium indicated by the stable readings from the aforementioned pore-water
224 pressure transducers.

225 Simulation of the excavation process was achieved by draining the heavy fluid from the void
226 between the former and latex bag. The rate of flow of the heavy fluid was set such that the entire
227 process took approximately three minutes. Data from the surface displacements, subsurface
228 displacements, pore-water pressure and heavy fluid pressure was taken at a rate of one per
229 second. Once all ground movements had stopped the model was decelerated and hand shear
230 vane readings were taken at various depths within the clay outside the zone of influence of the
231 shaft. These readings could be used to determine the undrained shear strength, S_u , for each
232 model. McNamara et al. (2011) demonstrated that, in this type of overconsolidated clay sample,
233 post-test shear vane readings taken in the far field provided measurements of S_u directly
234 comparable with in-flight measurements using a penetrometer and these readings are therefore

235 considered representative of the initial undrained shear strength of the sample. These results can
236 be found in Figure 4 along with the calculate variation in OCR.

237

238 RESULTS

239

240 *Correlation of test data*

241 Before any comparison of settlement data can be undertaken, it is necessary to ascertain the
242 similarity between each model. Aside from the differences in geometry, there are other
243 experimental factors that may influence the results obtained such as inconsistencies in undrained
244 soil strength and initial fluid level within the excavation (i.e. the horizontal pressure supporting the
245 soil around the shaft). The best fit lines to the measurements of undrained shear strength shown
246 in Figure 4 indicate that Test CR and EL1 show very similar undrained strength profiles (with
247 some expected scatter in the discrete readings) whereas Test EL2 is somewhat lower. For
248 example, at a depth of 100mm (i.e. half the depth of the shaft) the undrained strength of EL2 is
249 approximately 10% lower than CR and EL1. Pressure measurements within the heavy fluid also
250 showed that the initial fluid level within the excavation was around 20% higher in Test EL2
251 compared with that in Tests CR and EL1. These differences in initial conditions arise from the
252 complex nature of the apparatus and model preparation process but will clearly have an effect on
253 the measured results.

254 It is necessary to separate the effects on ground movements of these experimental variations
255 from the differences that arise from changing the geometry of the shaft and a method was devised
256 to account for the overall influence of the experimental variations. The presence of the stiff former
257 implies that the end position of the soil is known i.e. once the fluid is drained, the soil moves
258 (generally) horizontally until it comes into contact with the former. The effect of experimental
259 differences can therefore be quantified by measuring the horizontal movement of the soil
260 immediately adjacent to the shaft former as the fluid is drained. This movement must represent
261 the distance between the soil's initial position and the former. Figure 5 shows this data, obtained
262 from digital image analysis using geoPIV_RG (Stanier *et al.*, 2015). It is clear that the horizontal
263 movements in test EL2 are larger, indicating a bigger initial gap which is considered to be the
264 dominant factor in the measured surface movements upon excavation. The area under each

265 curve was obtained by numerical integration and it was found that (considering Test CR as the
266 reference case) test EL1 had horizontal movements that were 3% lower than the reference case
267 and test EL2 has movements that were 54% higher. This measurement can be considered to be
268 analogous to the concept of volume loss used in tunnelling. The rate of excavation in the test is
269 high and the event is essentially undrained. As such, the data for each test can be normalised to
270 account for the fact that the movements driving the observed mechanisms (i.e. the initial gap
271 between soil and former at the end of in-flight consolidation) are greater or smaller than the
272 circular reference case.

273

274 *Accounting for the effect of friction at the clay model and PMMA window interface*

275 In this paper, measurements of soil movements are presented from various areas of the model
276 and comprise surface settlement measurements obtained from 3D topography (Le *et al.*, 2016)
277 and front face, subsurface measurements from geoPIV_RG (Stanier *et al.*, 2015). Le *et al.* (2016)
278 demonstrated that both of these techniques were capable of making measurements with
279 comparable degrees of precision and accuracy. The (necessary) use of different measurement
280 techniques means that some correlation must take place as front face measurements obtained
281 from digital image analysis are influenced by friction between the soil and front window of the
282 strongbox. Grant (1998) examined this phenomenon in a series of experiments using clay
283 samples prepared in an identical manner to those in the current work and determined that an
284 offset of -0.1 mm was evident in the region of interest when comparing results from LVDTs and
285 image analysis. Put another way, Grant (1998) accounted for the friction at the clay-window
286 interface by adding 0.1 mm to the settlements taken from digital image analysis.

287 In the current work, the region of interest is larger than that considered by Grant (1998); his work
288 considered the movements immediately above a tunnel excavation. The application of an offset
289 was therefore deemed inappropriate in this case. The reported 0.1 mm correction of Grant (1998)
290 correlates to a scaling of around 10% and this scaling factor was therefore applied to
291 measurements made at the clay-window interface in the work presented here.

292 To summarise, all results obtained (i.e. from both measurement systems at all locations) were
293 scaled to account for variations in the experimental technique as previously detailed.

294 Subsequently, measurements made at the front face of the model were increased by 10% to
295 account for interface friction.

296

297 *Surface settlement data*

298 Once the corrections detailed above have been applied to tests EL1 and EL2 it is possible to
299 compare the surface settlements obtained parallel to the major and minor axes of the elliptical
300 shaft and compare them with the (axisymmetric) settlements generated by the circular shaft.
301 Figure 6 shows a sketch of the location of the measurement points and Figures 7a and 7b show
302 the comparison along the major and minor axes respectively. In these figures it should be noted
303 that those data labelled "P" (solid markers) are taken perpendicular to the front face of the
304 centrifuge strong box using 3D topography and those labelled "F" (open markers) are taken at the
305 front face both by geoPIV_RG and 3D topography (hence the larger number of data points).

306 The dashed lines are least squares best fits of Equation 2 to the data from the circular reference
307 test and the elliptical shaft tests. Data from the elliptical tests show good agreement independent
308 of the measuring technique used. Settlements along the major axis are significantly smaller than
309 those generated by the circular shaft excavation despite the major axis being 25% larger than the
310 diameter of the circle (100mm vs 80mm). Conversely, settlements along the minor axis are
311 comparable with those generated by the circular excavation despite the minor axis being 20%
312 smaller than the diameter of the circle.

313

314 DISCUSSION

315

316 *The nature of the modelled shaft*

317 It should be noted that the normalised settlements presented from the current tests are very much
318 larger (by an order of magnitude) than those observed in the field (New, 2017). This arises from
319 the fact that, in these tests, there is a 300mm overcut (at prototype scale) between the soil and
320 the permanent former. As previously discussed, this is very much larger than that which might
321 be encountered in practice where a 100mm overcut that is subsequently grouted might be more
322 reasonable. The large overcut is an artifact of the experiments deliberately chosen to ensure
323 consistent movements that can be reliably detected by digital image correlation.

324 The heavy fluid within the excavation is drained via a pipe embedded within the soil attached to
325 the base of the latex bag. It might be expected that the presence of this pipe would have some
326 influence on the ground movements however it is located on the centreline of the excavation. As
327 this is also aligned with a plane of symmetry, movements in this area would be expected to be in
328 the form of vertical heave only and would be less influenced by the smooth pipe, in itself aligned
329 with the direction of heave. Post-test inspection shows that the pipe and latex bag have very little
330 effect on the heave at the formation and what influence there is occurs only when the soil is fully
331 softened at the base i.e. some time after the end of excavation simulation.

332

333 *Comparison with empirical methods*

334 Figure 8 shows that the surface settlements generated by the elliptical shaft excavation could be
335 represented by Equation 1 (New, 2017). A least squares best fit to the combined data (i.e. from
336 all tests and measurement methods) is carried out to determine values of α and n . Figure 8 shows
337 the resulting curves and Table 2 gives the derived values of α and n .

338

339 *Comparison with the results of Faustin et al. (2018)*

340 As detailed earlier there is one previously published set of experimental data detailing a centrifuge
341 test on an elliptical shaft constructed in dense sand. Despite the differences between this and
342 the current work, Equation 2 is utilised to examine the patterns of movement generated. Figure
343 9 shows the results from Faustin *et al.* (2018) overlain with predicted curves generated by
344 Equation 2. The curves are not mathematically fit to the data but rather placed to give an
345 approximate upper bound to the data on the graph. The curve generated for the elliptical data
346 has a value of α that is 10% larger than that used for the circular curve (the value of n is constant
347 at 1.5). This is commensurate with the observation that the plan area of the elliptical shaft is 10%
348 larger in this work when compared with the circular. The curves give credence to the observation
349 above that a suitable prediction can be generated for the maximum settlements caused by
350 excavating an elliptical shaft from Equation 2 by considering a circular shaft of equivalent plan
351 area. It should be noted that in the current work, the aspect ratio of the ellipse is 0.64 (and 0.67
352 in Faustin *et al.*, 2018). Whether similar patterns of settlement would be observed for different
353 aspect ratios remains a topic for future work.

354

355 CONCLUSION

356

357 A practical solution to the problem of restrictions on available surface space coupled with
358 increasingly congested underground space is the utilisation of elliptical shafts for access to
359 underground infrastructure. It is clear that there is a requirement for estimating the ground
360 movements resulting from such constructions and data from a series of well-controlled centrifuge
361 tests carried out in overconsolidated clay have been presented in this paper.

362 The findings can be summarised below:

- 363 • The maximum settlements at the ground surface arising from elliptical shaft construction
364 are apparent on line coincident with the minor axis of the ellipse. Conversely, the
365 settlements generated on the line coincident with the major axis are significantly smaller
366 in magnitude (in the order of 60% of the settlement seen on the minor axis, for the ratio
367 in lengths of the minor to major axis of 0.64).
- 368 • For the purposes of assessing the movements that might be generated by a proposed
369 elliptical shaft construction in clay, an upper bound to the surface settlements can be
370 generated from Equation 2 by modelling a circular shaft of equivalent plan area. As with
371 the original work of New & Bowers (1994) special consideration will still need to be given
372 to an appropriate value of α .

373

374 ACKNOWLEDGEMENT

375

376 The authors gratefully acknowledge the support of the Leverhulme Trust (Grant no. RPG-2013-
377 85).

378 REFERENCES

379

380 Allenby, D. & Kilburn, D. (2015) Overview of underpinning and caisson shaft-sinking techniques.

381 Proceeding of the Institution of Civil Engineers – Geotechnical Engineering, Vol. 168, No.

382 1, pp. 3-15.

383 British Standards Institution (2007). BS EN 1997-2:2007 Euro-code 7: Geotechnical Design.

384 Ground investigation and testing. BSI, London, UK.

385 Divall, S. & Goodey, R.J. (2016). An apparatus for centrifuge modelling of a shaft construction in

386 clay. In L. Thorel, A. Bretschneider, M. Blanc, & S. Escoffier (Eds.), *3rd European*

387 *Conference on Physical Modelling in Geotechnics (Eurofuge 2016)* Vol. 1 (pp. 307-312),

388 Nantes, France.

389 Faustin, N.E. (2017). Performance of circular shafts and ground behaviour during construction.

390 PhD Thesis, Cambridge University, Cambridge, UK

391 Faustin, N.E., Elshafie, M.Z.E.B. & Mair, R.J. (2018). Modelling the excavation of elliptical shafts

392 in the geotechnical centrifuge. Proceedings of the 9th International Conference on

393 Physical Modelling in Geotechnics, Vol 2, pp. 791-796. London, UK.

394 Feiersinger, A. (2011). Comparison of deformations predicted using 3D finite element analysis

395 with deformations encountered during construction. The Harding Prize Competition,

396 British Tunnelling Society.

397 Grant, R.J. (1998). Movements around a tunnel in the two-layer ground. PhD thesis, City,

398 University of London, UK.

399 Le, B.T., Goodey, R.J. & Divall, S. (2019). Subsurface ground movements due to circular shaft

400 construction. *Soils and Foundations*, Vol. 59, No. 5, pp. 1160-1171.

401 Le, B.T., Nadimi, S., Goodey, R.J. & Taylor, R.N. (2016). System to measure three-dimensional

402 movements in physical models. *Géotechnique Letters*, Vol. 6, No. 4, pp. 256-262.

403 McNamara, A.M., Rettura, D., & Gorasia R.J. (2011). Press-In Engineering, Proceedings of 3rd

404 International Workshop, Shanghai, pp 25-31.

405

406 Morrison, P.R.J., McNamara, A.M. & Roberts, T.O.L. (2004). Design and construction of a deep
407 shaft for Crossrail. *Proceedings of the Institution of Civil Engineers – Geotechnical*
408 *Engineering*, Vol. 157, No. 4, pp. 173–182.

409 New, B. (2017). Settlements due to shaft construction. *Tunnels and Tunnelling International*,
410 September 2017, pp. 16-17.

411 New, B.M. & Bowers, L.K. (1994) Ground movement model validation at Heathrow Express trial
412 tunnel, *Tunnelling '94*. London, UK.

413 Panchal, J.P. (2018). Minimising ground movements around deep excavations in soft soils. PhD
414 Thesis, City, University of London, London, UK

415 Pedro, A.M. (2013). Geotechnical investigation of IVENS shaft in Lisbon. PhD Thesis, Imperial
416 College, London, UK.

417 Psomas, S., Coppenhall, P., Rimes, M., Brown, D. & Cheevers, E. (2019). Design and
418 construction of permanent steel fibre reinforced sprayed concrete lining shafts for the
419 Thames Tideway Tunnel project UK. *Proceedings of the World Tunnel Congress 2019*,
420 Naples, Italy.

421 Ritty, P., Bedi, A., Hsu, Y.S., Heath, I. & Mimmagh, F. (2015). Design and construction of a spray
422 concrete lined shaft adjacent to running tunnels. *Proceedings of the 16th European*
423 *Converence on Soil Mechanics and Geotechnical Engineering*, Vol. 2, pp. 509-514.
424 Edinburgh, UK.

425 Schwamb, T. (2014) Performance Monitoring and Numerical Modelling of a Deep Circular
426 Excavation. PhD Thesis, Cambridge University, Cambridge, UK. Stanier, S.A., Blaber, J.,
427 Take, W.A. and White, D.J. (2015). Improved image-based deformation measurement
428 for geotechnical applications. *Canadian Geotechnical Journal*, Vol. 53, No. 5, pp. 727-
429 739.

430 Topa Gomes, A., Silva Cardoso, A., Almeida e Sousa, J. Andrade, J. & Campanhã, C. (2008).
431 Design and behaviour of Salgueiros station for Porto Metro. *Proceedings of the 6th*
432 *International Conference on Case Histories in Geotechnical Engineering*, Vancouver,
433 USA.

434

435 LIST OF FIGURES

436

437 **Figure 1:** Sketch showing required circular and elliptical plan geometry to enclose two adjacent
438 lift mechanisms.

439 **Figure 2:** Photographs of apparatus showing: (top) assembly of former, latex bag and bracket,
440 (middle) location of apparatus within the soil model, (bottom) attachment of the apparatus to the
441 model box.

442 **Figure 3:** Schematic of centrifuge test apparatus.

443 **Figure 4:** Undrained shear strength with depth for CR, EL1 and EL2.

444 **Figure 5:** Horizontal displacement with depth for CR, EL1 and EL2 (L: results from left side of
445 model, R: results from right side).

446 **Figure 6:** Sketch to show measurement locations.

447 **Figure 7a:** Comparison of surface settlements in elliptical shaft test (EL) along the major axis
448 direction with reference circular shaft data (CR).

449 **Figure 7b:** Comparison of surface settlements in elliptical shaft test (EL) along the minor axis
450 direction with reference circular shaft data (CR).

451 **Figure 8:** Design lines for surface settlements arising for elliptical shaft construction in clay.

452 **Figure 9:** Comparison of Equation 2 with the results of Faustin (after Faustin *et al.*, 2018)

453

1

Test ID	Maximum consolidation pressure (kPa)	Swelling pressure (kPa)	Excavation dimensions (mm or mm ²)	Shaft liner dimension (mm or mm ²)
CR (aspect ratio = 1.0)	350	250	h = v = 80 H = 200 A = 5027	h = v = 71 H = 200 A = 3959
EL1 (aspect ratio = 0.64)	350	250	h = 64 v = 100 H = 200 A = 5027	h = 55 v = 45.8 H = 200 A = 3959
EL2 (aspect ratio = 0.64)	350	250	h = 100 v = 64 H = 200 A = 5027	h = 91.6 v = 55 H = 200 A = 3959

2 **Table 1:** Details of centrifuge tests

3

Test	CR	EL1	EL2 ⁴
α	5.8×10^{-3}	4.1×10^{-3}	5.9×10^{-3}
n	1.5	0.94	1.33

6 **Table 2.** The values of α and n derived from the tests.

7

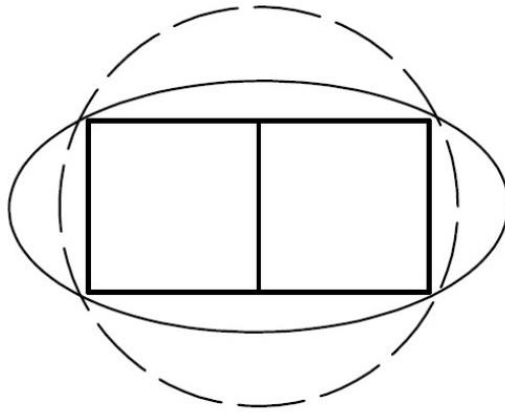


Figure 1: Sketch showing required circular and elliptical plan geometry to enclose two adjacent lift mechanisms.

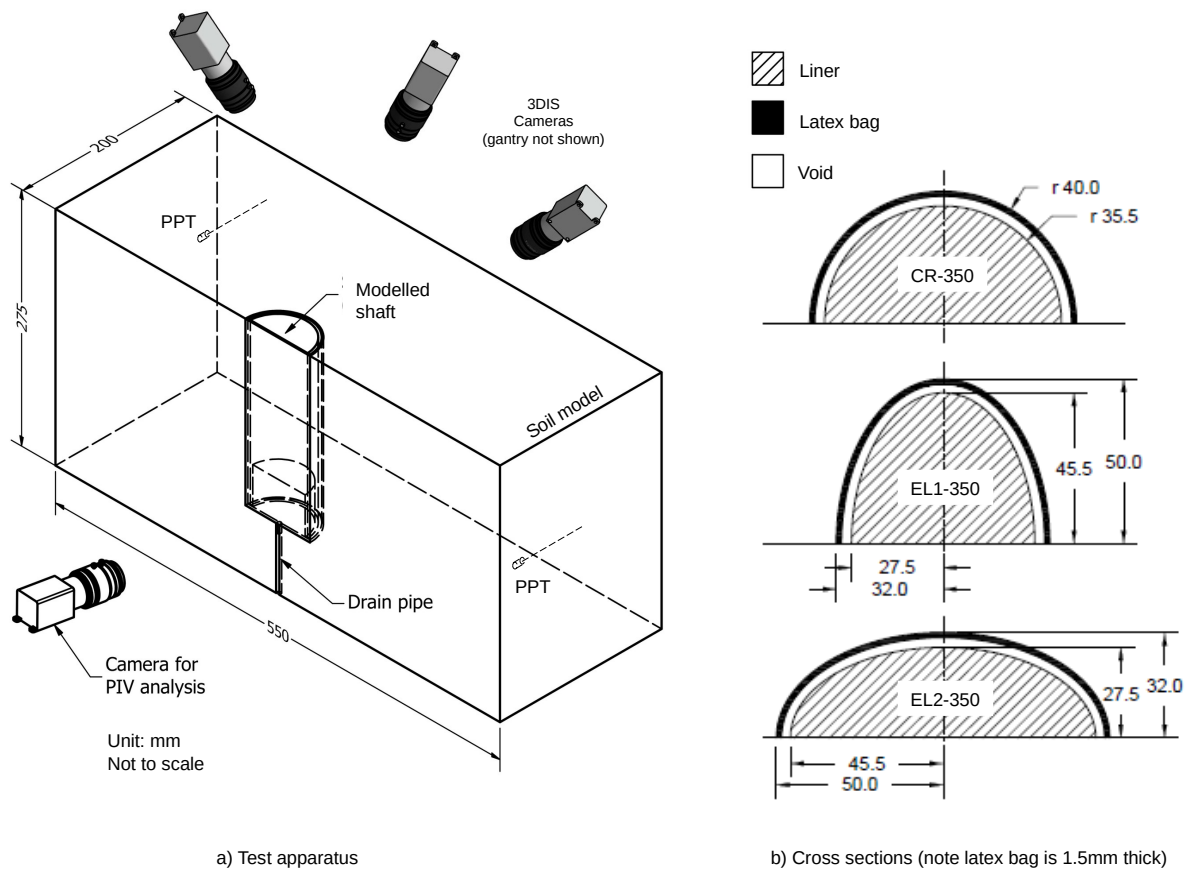


Figure 2: Schematic of centrifuge test apparatus.

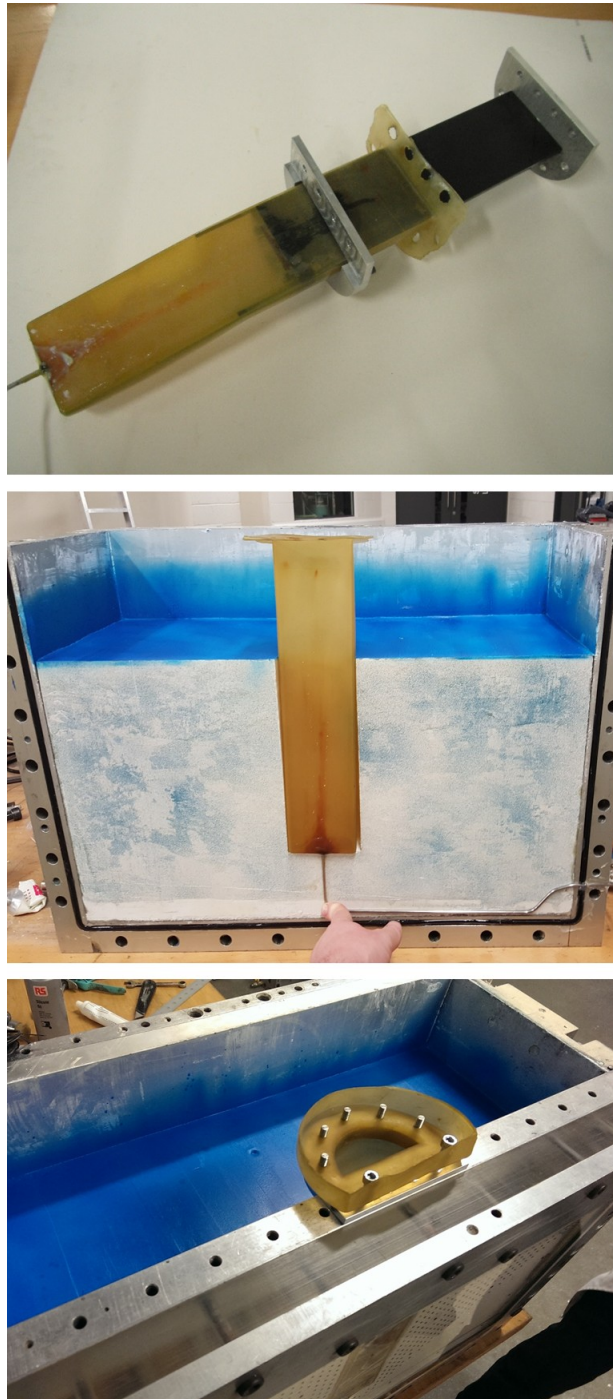


Figure 3: Photographs of apparatus showing: (top) assembly of former, latex bag and bracket, (middle) location of apparatus within the soil model, (bottom) attachment of the apparatus to the model box.

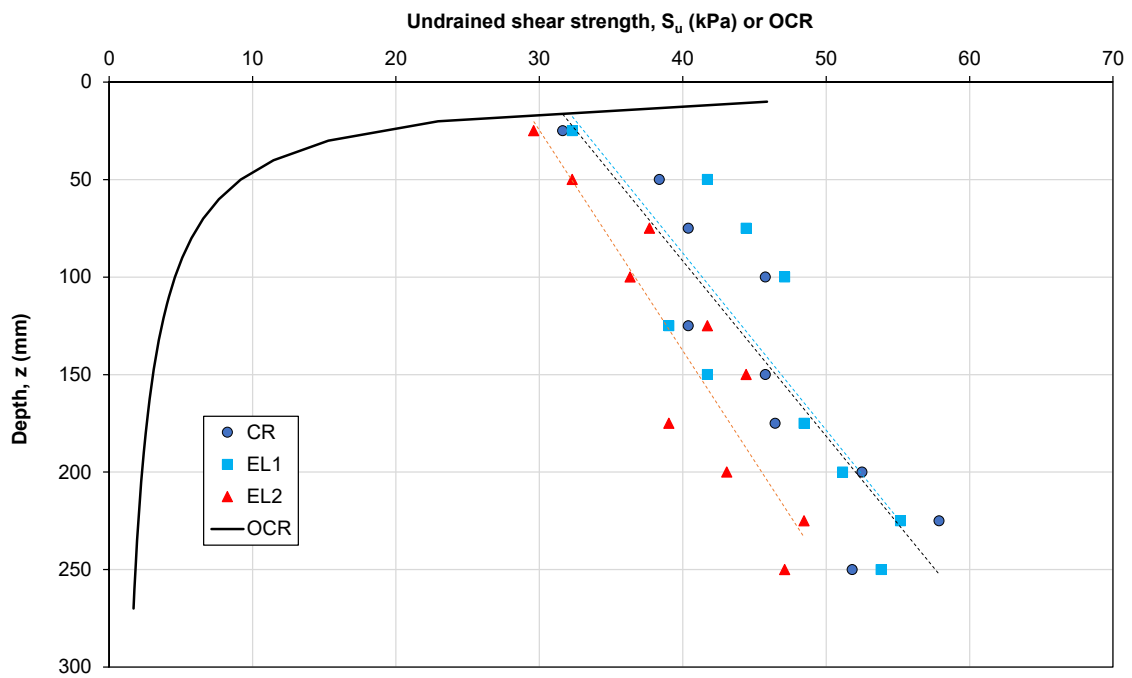


Figure 4: Undrained shear strength and OCR with depth for CR, EL1 and EL2.

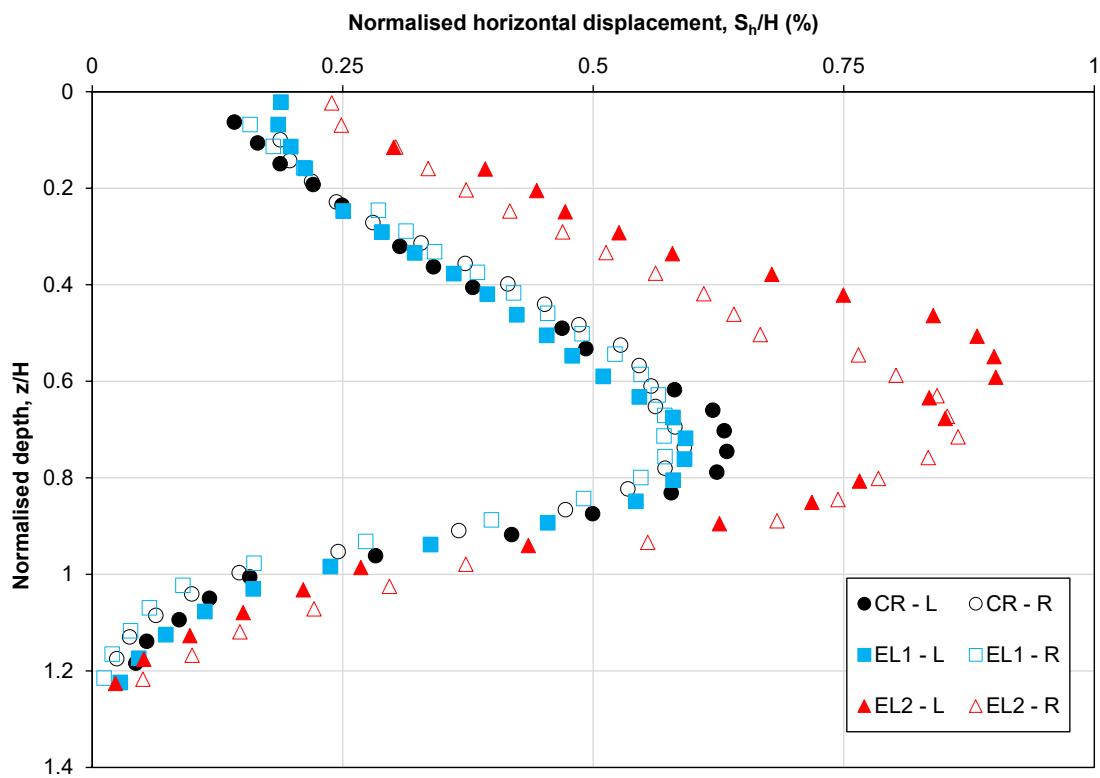


Figure 5: Horizontal displacement with depth for CR, EL1 and EL2 (L: results from left side of model, R: results from right side).

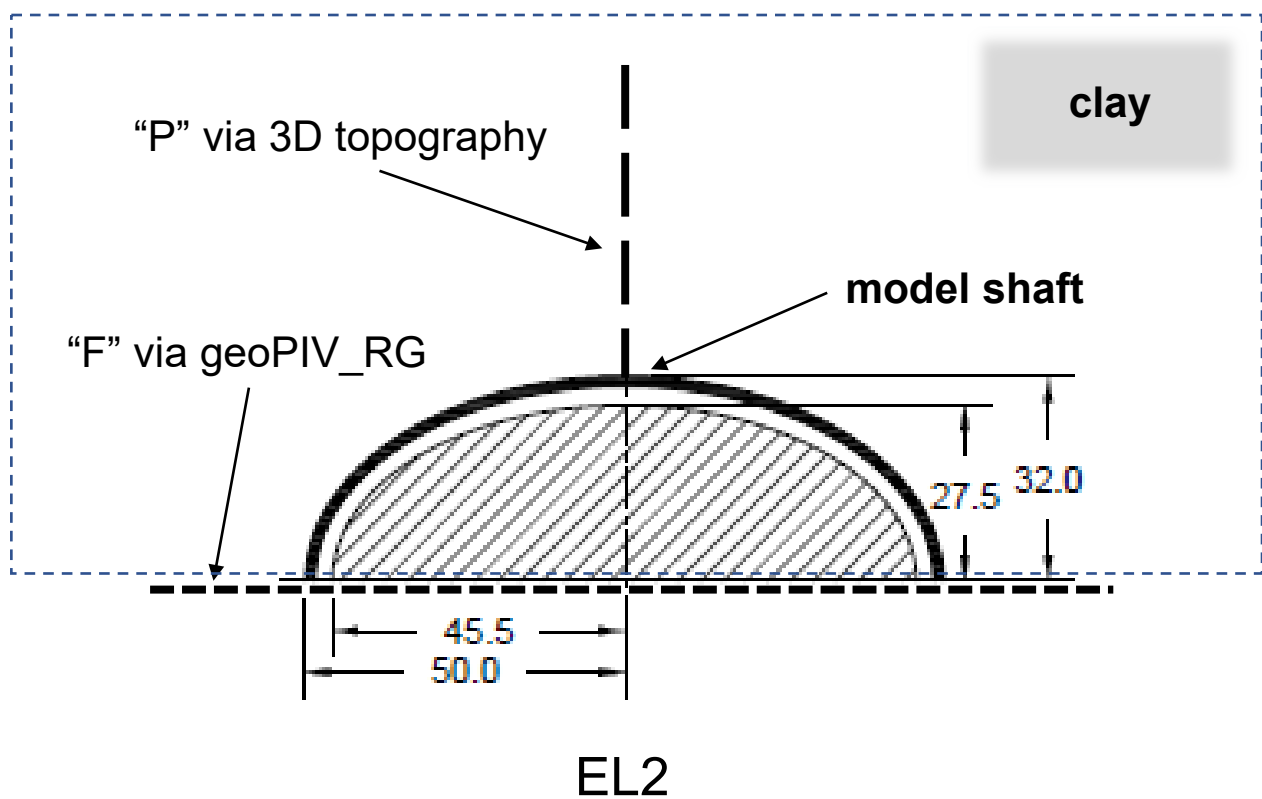
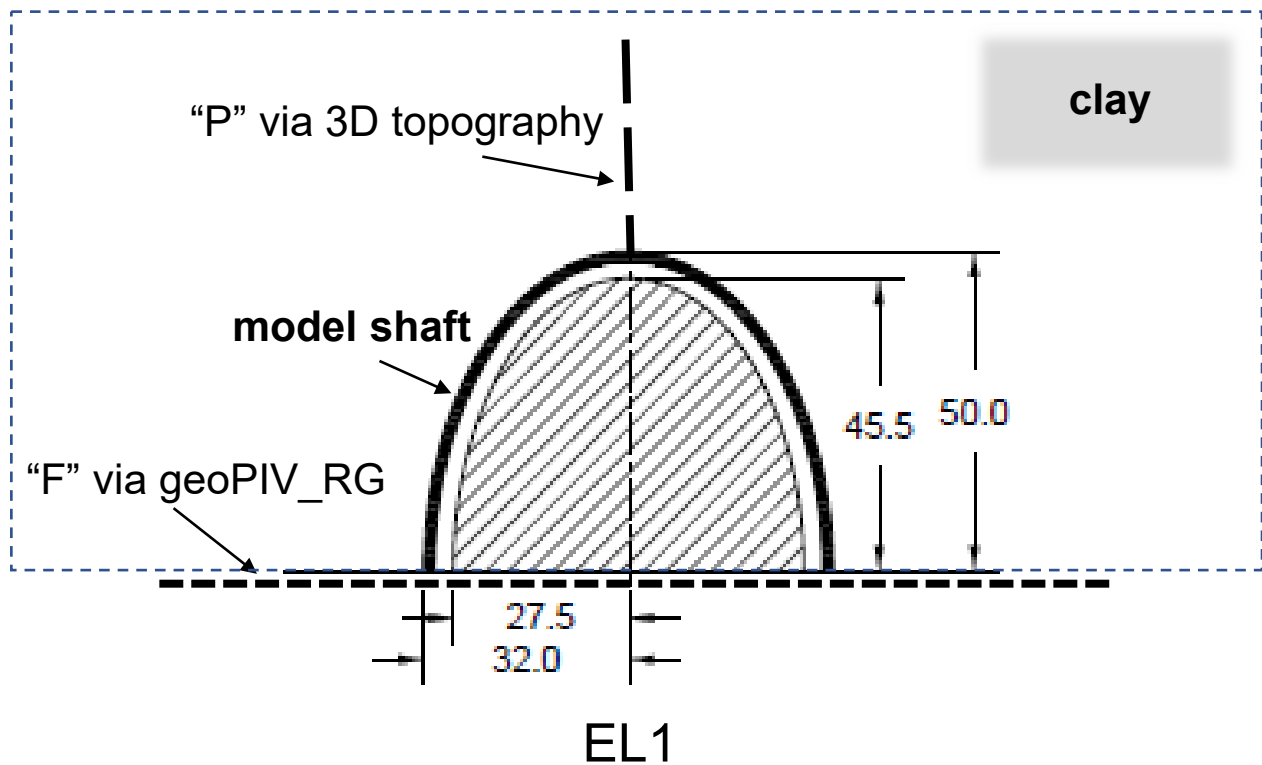


Figure 6: Sketch to show measurement locations

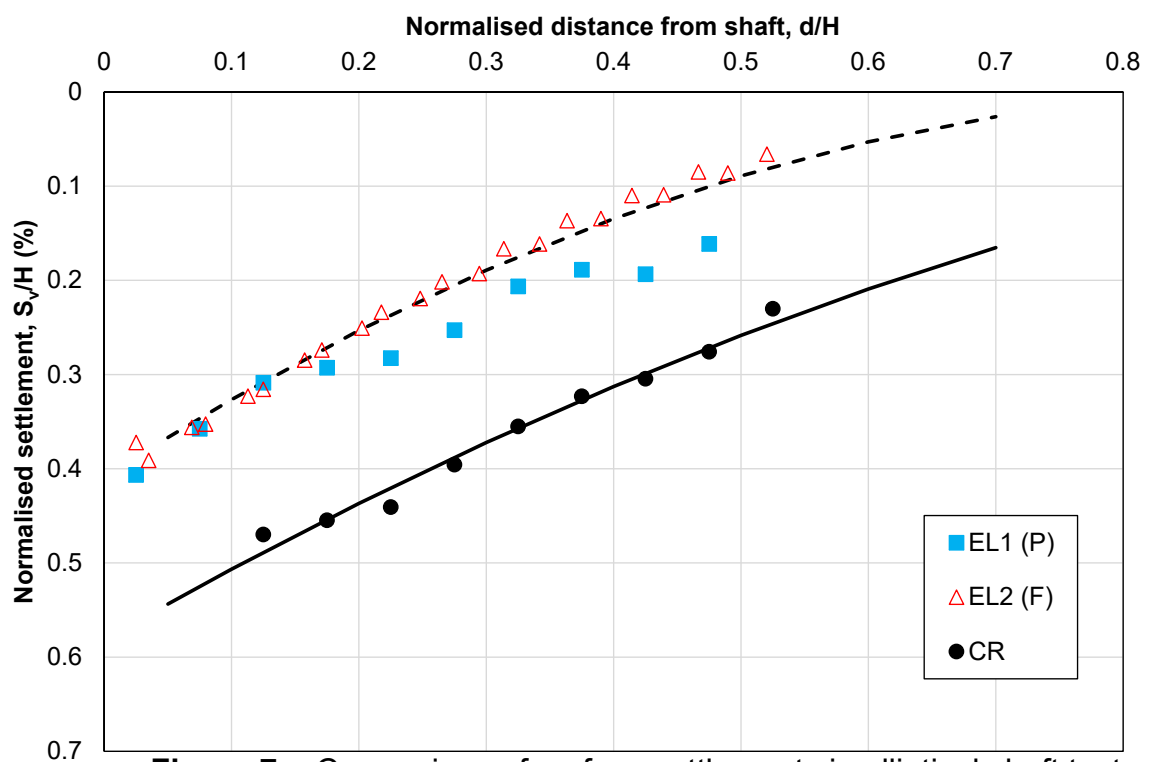


Figure 7a: Comparison of surface settlements in elliptical shaft test (EL) along the major axis direction (CR) with reference circular shaft data (CR).

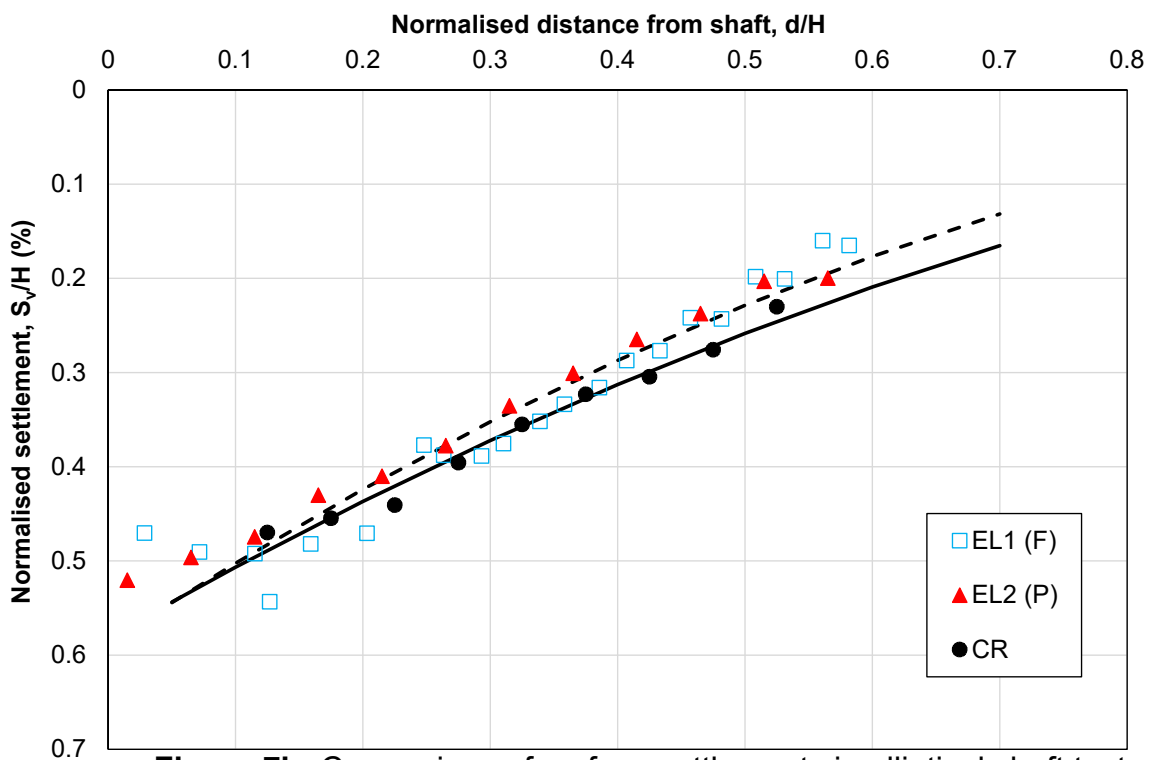


Figure 7b: Comparison of surface settlements in elliptical shaft test (EL) along the minor axis direction (CR) with reference circular shaft data (CR).

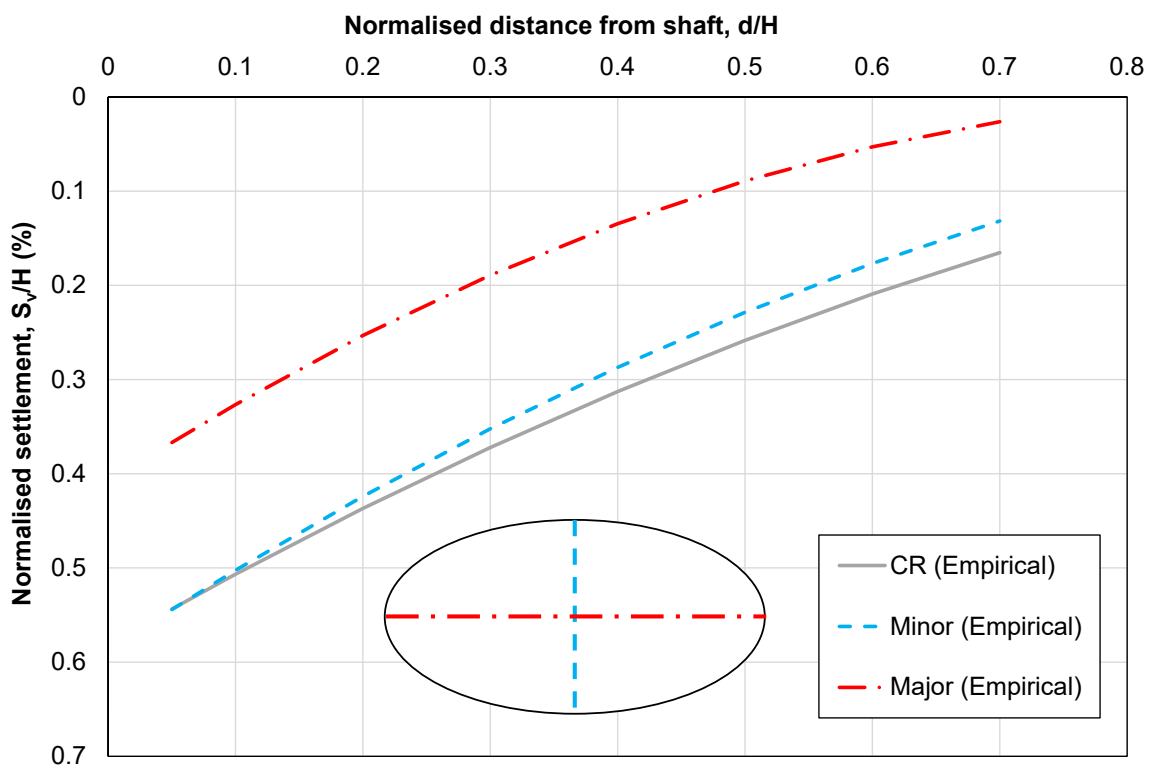


Figure 8: Design lines for surface settlements arising for elliptical shaft construction in clay.

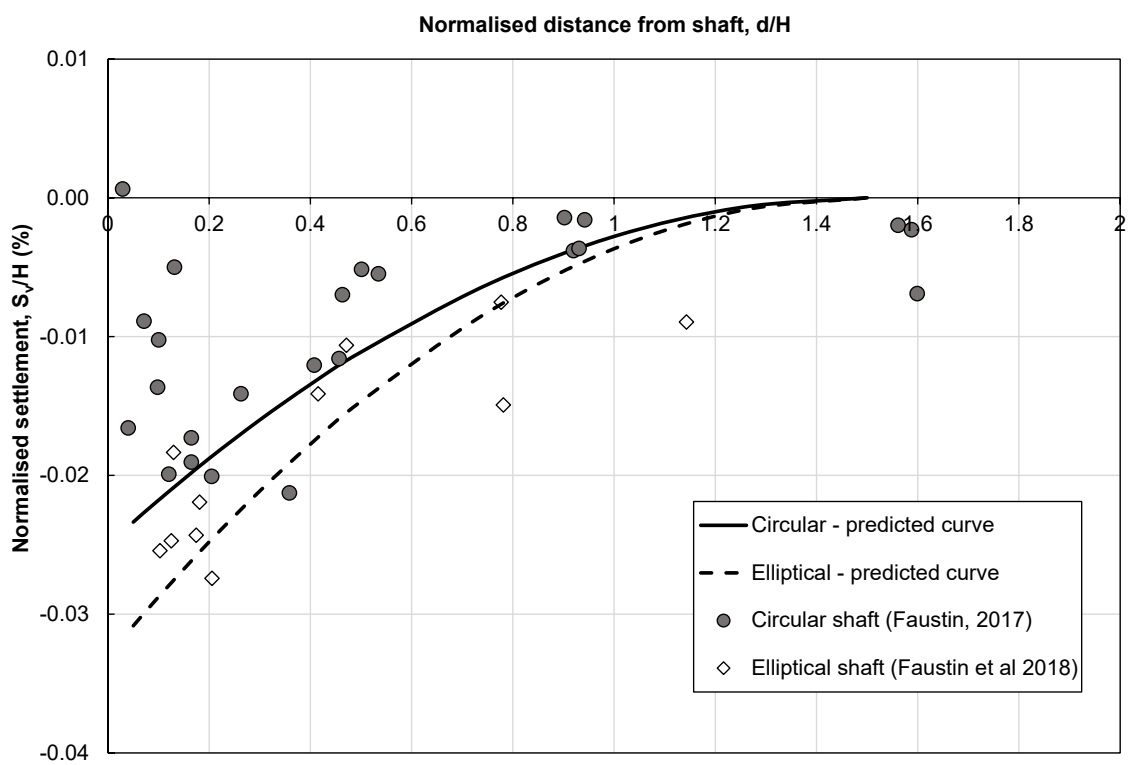


Figure 9: Comparison of Equation 2 with the results of Faustin (after Faustin *et al.*, 2018)